Expression of Osteopontin in M2 and M4 Intrinsically Photosensitive Retinal Ganglion Cells in the Mouse Retina

Leonie Kinder[1] and Moritz Lindner[1–3]

[1]Institute of Physiology and Pathophysiology, Department of Neurophysiology, Philipps-University, Marburg, Germany
[2]The Nuffield Laboratory of Ophthalmology, Sleep and Circadian Neuroscience Institute, Nuffield Department of Clinical Neurosciences, University of Oxford, Oxford, United Kingdom
[3]Department of Ophthalmology, Philipps-University, University Hospital of Giessen and Marburg GmbH, Marburg Campus, Marburg, Germany

Correspondence: Moritz Lindner, Institute for Physiology and Pathophysiology, University of Marburg, Deutschhausstraße 2, Marburg 35037, Germany; moritz@lindnerlab.de.

Received: October 31, 2024
Accepted: January 12, 2025
Published: February 5, 2025

Citation: Kinder L, Lindner M. Expression of osteopontin in M2 and M4 intrinsically photosensitive retinal ganglion cells in the mouse retina. *Invest Ophthalmol Vis Sci.* 2025;66(2):14. https://doi.org/10.1167/iovs.66.2.14

Purpose. Melanopsin-expressing intrinsically photosensitive (ip) retinal ganglion cells (RGCs) can be divided into six different subtypes (M1 – M6). Yet, specific markers exist for only some of these subtypes that could be employed to study the function of individual subtypes. Osteopontin (*Spp1*) marks αRGC, suggesting that, across ipRGCs, it would only mark the M4-ipRGC subtype (synonymous to ON-sustained αRGCs). Recent evidence suggests that osteopontin expression could spread to other ipRGC subtypes. Therefore, this study aims to characterize the expression pattern of osteopontin across ipRGC subtypes in mice.

Methods. Single-cell RNA (scRNA-seq) sequencing data from murine RGCs were analyzed to identify expression patterns of *Spp1* across ipRGCs. Immunohistochemistry (IHC) was performed on retinal cryosections and flatmounts from C57BL/6J mice to characterize the localization of osteopontin across ipRGCs. Neurite tracing was employed to study dendritic morphology and identify individual ipRGC subtypes.

Results. scRNA-seq analysis revealed *Spp1* expression in two distinct clusters of ipRGCs. IHC confirmed osteopontin colocalization with neurofilament heavy chain, an established marker for αRGCs, including M4-ipRGCs. Spp1 immunoreactivity was moreover identified in one additional group of ipRGCs. By dendritic morphology and stratification, those cells were clearly identified as M2-ipRGCs.

Conclusions. Our findings demonstrate that osteopontin is expressed in both M2- and M4-ipRGCs, challenging the notion of osteopontin as a marker exclusively for αRGCs. IHC double-labeling for osteopontin and melanopsin provides a novel method to identify and differentiate M2 ipRGCs from other subtypes. This will support the study of ipRGC physiology in a subtype -specific manner and may, for instance, foster research in the field of optic nerve injury.

Keywords: ipRGC, m2, m4, αRGC, osteopontin, spp1, melanopsin, retinal ganglion cells

In the mammalian retina, visual information is processed in more than 40 parallel pathways represented by dedicated subtypes of retinal ganglion cells (RGCs).[1,2] Based on functional commonalities, these subtypes can be classified into different overlapping groups, like the intrinsically photosensitive retinal ganglion cells (ipRGCs) or the αRGCs. Some RGC subtypes exhibit characteristics that align with multiple groups, leading to their classification within more than one of these groups. This is the case, for instance, for the M4-ipRGC subtype, which has been found to be identical with the ON-sustained subtype of αRGCs.[3]

ipRGCs received major attention after they had been discovered to express the opsin melanopsin (encoded by *Opn4*), which renders them intrinsically light responsive.[4–6] ipRGCs have since been found to mediate a range of non-image -forming responses to light, including circadian entrainment or pupil constriction. More recently, it has become clear that these cells also contribute to image-forming tasks, for instance, by adjusting contrast sensitivity.[7,8] This diversity of tasks is not mediated by all ipRGCs equally; rather, the different subtypes, termed M1 to M6, appear to be functionally specialized. M1 to M6 ipRGCs can be distinguished based on their *Opn4* expression level, cell morphology, and central projection patterns.[8,9] Key features are schematically summarized in Figure 1.

Numerous attempts have been made to associate specific ipRGC-mediated physiological functions with individual subtypes. These attempts have been particularly successful in cases where specific immunohistochemical or genetic markers existed to efficiently segregate the subtype of interest from the others. For instance, it has been shown that a specific subpopulation of M1 ipRGCs (those lacking *Brn3b* expression) is essential for circadian entrainment.[4,10] M4 cells are involved in setting contrast sensitivity[11] and M6

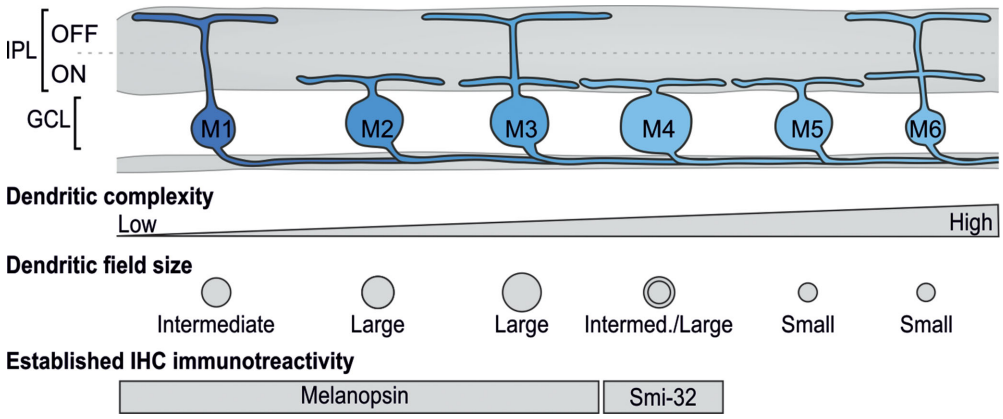

Figure 1. Schematic of the subtypes of ipRGCs and their structural features. The expression of melanopsin decreases from M1 to M6 (*blue*). M1 ipRGCs are the only subtype stratifying solely in the OFF lamina of the inner plexiform layer (IPL) while M2, M4, and M5 stratify in the ON lamina and M3 and M6 are bistratifying. Complexity of the dendritic tree increases from the M1 to M6 subtype. M2/M3 cells have the largest dendritic fields while those of M5 and M6 are small and M1/M4 intermediate. Only M1 to M3 ipRGCs express sufficient melanopsin to be detectable by standard immunohistochemical techniques. M4 cells are immunoreactive for the Smi-32 antibody (labeling unphosphorylated neurofilament heavy chain). For review, see Aranda and Schmidt.[7] GCL, ganglion cell layer.

likely in pattern vision.[12] Yet, *Brn3b*$^-$ M1, M4, and M6 cells are, to the best of our knowledge, the only ipRGC subtypes for which such markers have been identified, and the functional study of the remaining types still relies on laborious approaches like dye-filling during patch -clamp experiments.[13] Such methods might not enable functional assessment up to a behavioral level.

Thus, identification and careful characterization of potential markers is warranted to enable and accelerate functional characterization of the individual ipRGC subtypes. In this regard, osteopontin (also known as secreted phosphoprotein-1 [Spp1]), a multifunctional protein involved in intracellular and extracellular signaling, has caught our attention.[14] Osteopontin has long been considered a pan-αRGC marker,[15–17] which would imply that, among the ipRGCs, the M4 subtype should be the only one expressing relevant amounts of osteopontin. In a more recent study, it has been observed that osteopontin immunoreactivity spreads beyond αRGCs, particularly into cells that are also immunopositive for melanopsin (i.e., M1–M3 ipRGCs; Fig. 1).[18] If osteopontin expression was defined to one specific subtype among the M1 to M3 ipRGCs, this might open room for specific immunohistochemical or transgenic labeling, which could facilitate segregating the specific functional roles of M1 to M3 cells. This is especially true as mouse lines exist that express Cre recombinase under control of the *Spp1* promoter (MGI: 6450712), which would enable flexibly manipulating this subtype. Moreover, understanding how osteopontin expression exactly spreads beyond αRGCs could help to further clarify its potential role in supporting RGC resilience against axonal injury[15] and glaucomatous damage,[18,19] which a large recent study suggests could be a feature more strongly associated with ipRGCs than with αRGCs.[2]

In this study, we therefore examine the expression pattern of osteopontin across ipRGC subtypes using a set of transcriptomic and immunohistochemistry (IHC) techniques. We find that osteopontin expression outside αRGCs is confined to the M2 subtype of ipRGCs, and the combination of high osteopontin and clear melanopsin immunoreactivity may thereby facilitate the identification of this subtype.

Material and Methods

Animals

C57BL/6J mice were purchased from Charles River Laboratories (Sulzfeld, Germany). Handling of the mice and tissue collection was performed in accordance with the federal and institutional guidelines.

Tissue Preparation

For histologic analysis, mice were culled by decapitation under isoflurane anesthesia, and tissue was collected and processed following in-house standard procedures.[20] Eyes were punctured with a fine-gauge needle, fixed in 4% methanol-free paraformaldehyde (Thermo Fisher, Waltham, MA, USA) in phosphate-buffered saline (PBS) for 30 minutes (cryosections) or 24 hours (flatmounts), and then transferred to 30% sucrose in H_2O. For preparation of retinal cryosections, eyes were embedded into Optimal Cutting Temperature (OCT) medium (VWR, Lutterworth, UK) and stored at −80°C until further processing. Then, 18-µm tissue sections were prepared using a CM1850 Cryotome (Leica, Wetzlar, Germany). For retinal flat mount preparation, the anterior segment of the fixed eye was removed by cutting posterior to the ora serrata, and the retina was mobilized by gently lifting it off from the underlying RPE with sclera. Four releasing incisions were made into the retina before storing it in PBS until further use.

Immunohistochemistry

Fluorescent immunolabeling was performed using standard techniques as previously described.[20] Briefly, retinal cryosections were permeabilized in PBS with 0.2% Triton-X (PBSTX-0.2). Blocking was performed in PBSTX-0.2 with 10% normal donkey or goat serum (Sigma-Aldrich, St. Louis, MO, USA). Sections were then incubated with primary antibodies for 24 hours at 4°C and after washing with 0.1% Tween in PBS incubated with secondary antibodies for another 2 hours at room temperature. Sections were mounted with Prolong Gold antifade media (Life Technologies/Thermo Fisher Scientific,

Investigative Ophthalmology & Visual Science

Table. List of Primary and Secondary Antibodies Used in This Study

Target	Host	Antibody	Dilution
Primary antibodies			
Osteopontin (SPP1, OPN)	Mouse	SantaCruz Biotechnology sc-73631 RRID:AB_2194995	1:1000–1:2000
Melanopsin (Opn4)	Rabbit	Advanced Targeting Systems AB-N39 RRID:AB_1608076	1:2000
Neurofilament heavy polypeptide (Smi-32)	Chicken	Abcam ab4680 RRID:AB_304560	1:8000-1:10000
Secondary antibodies			
Mouse	Donkey	Invitrogen Alexa Fluor 488 Cat#A-21202 RRID:AB_141607	1:500–1:2000
Rabbit	Donkey	Invitrogen Alexa Fluor 488 Cat#A-21206 RRID:AB_2535792	1:500–1:2000
Chicken	Goat	Invitrogen Alexa Fluor 568 Cat#A-11041 RRID:AB_2534098	1:500–1:2000
Mouse	Donkey	Invitrogen Alexa Fluor 568 Cat#A-10037 RRID:AB_11180865	1:500–1:2000
Rabbit	Goat	Invitrogen Alexa Fluor 633 Cat#A-21050 RRID:AB_2535718	1:500–1:2000

Carlsbad, CA, USA). All antibodies were diluted in PBSTX-0.2 containing 2.5% normal donkey serum.

For flat mount staining, 1% Triton-X in PBS (PBSTX-1) was used for permeabilization. Blocking was performed in PBSTX-1 with 10% normal donkey or goat serum (Sigma-Aldrich). Primary antibody incubation was performed over 3 days at room temperature, followed by incubation with the second antibody overnight at room temperature. Washing steps were performed in 0.1% Tween in PBS. Antibody soles were made up in PBSTX-1 with 2.5% normal donkey/goat serum. A list of all primary and secondary antibodies used in this study is given in the Table.

Image Acquisition and Analysis

Fluorescence images were acquired using an upright LSM 710 laser scanning confocal microscope (Zeiss, Oberkochen, Germany) equipped with a 40× oil objective (NA = 1.3). Laser lines for excitation were 405 nm, 488 nm, 561 nm, and 633 nm with emissions collected 440 to 480 nm, 505 to 550 nm, 580 to 625 nm, and >640 nm, respectively. Individual channels were collected sequentially. Image postprocessing was restricted to global enhancement of brightness and contrast, as well as cropping, downscaling, and subselecting of fluorescent channels as required. Post processing was performed using ImageJ/FIJI (National Institutes of Health, Bethesda, MD, USA).[21] For retinal flatmounts, Z-stacks (slice interval 0.45 µm, average depth: 16.87 ± 1.36 µm) were acquired from four adjacent areas and were stitched together using FIJI's three-dimensional (3D) stitching tool[22] to ensure coverage of the entire dendritic field of any neuron in the center of the stitched image. The ImageJ plugin Simple Neurite Tracer was used for semiautomatic neuron tracing.[23] Per stitched composite image, at least one index (osteopontin$^+$/melanopsin$^+$) and one control cell (osteopontin$^-$/melanopsin$^+$) were traced, and signal intensity, number of branching points, and dendritic field area were quantified. Signal intensity was quantified as the mean pixel intensity in a 3D region of interest covering the soma of the cell under investigation. As neither laser stimulus intensity nor acquisition parameters were normalized, intensity values were calculated as relative to a control cell on the same image.

Bioinformatics

To characterize the transcriptomic profile of the individual ipRGC subtypes, a publicly available single-cell RNA sequencing (scRNA-seq) data set[2] was analyzed. Gene count matrices were obtained from the Gene Expression Omnibus (GEO) server, www.ncbi.nlm.nih.gov/geo/ (accession number GSE137863). Processing and analyzing of the data set were performed using the R software environment (version 3.5.1) and the Seurat package (version 5).[24,25] Clustering was performed after dimensionality reduction by Seurat's inbuilt shared nearest neighbor modularity optimization-based clustering algorithm.

Results

To explore the expression pattern of osteopontin in ipRGCs, we harnessed a publicly available sc RNA-seqdata set from retinal ganglion cells.[2] We first identified melanopsin/*Opn4*-expressing cells in this data set ($n = 2211$) and selected those for further analysis. Unsupervised clustering revealed six transcriptomically distinct populations of ipRGCs (Fig. 2A). We then used *Opn4* expression levels as well as expression levels for *Nefh* (coding for neurofilament heavy chain protein, characteristic for M4 cells[3]), *Gna14* (coding for the G-protein $G_{14}\alpha$, shown to be functional in M1 > M3),[26] and *Hcn1/2* (coding for two hyperpolarization-activated cyclic nucleotide-regulated ion channels, relevant for signal transduction in M4, less so in M2 and M3 but not in M1)[26] to assign these clusters to the previously described ipRGC subtypes (Figs. 2B, 2C). Probing for *Spp1* expression in those clusters, we found that *Spp1* expression was highest in the cluster presumably representing M2 cells while expression levels detected in the cluster representing M4 cells were markedly lower (log2-fold change = 2.15, $P < 0.001$, Figs. 2C–E).

To probe whether these transcript-level observations would be reflected at the protein level, we continued our analysis performing IHC staining on retinal cryosections. We performed triple labeling for osteopontin together with Smi-32 (labeling unphosphorylated neurofilament heavy chain) as a bona-fide pan-marker for αRGCs, including M4[3,16,27,28] and melanopsin, to identify M1 to M3 ipRGCs. The results showed the previously reported colocalization of Smi-32 and osteopontin in the ganglion cell layer. These Smi-32$^+$/osteopontin$^+$ cells appeared to have rather large somas, consistent with the assumption that these would be αRGCs (Figs. 3A, 3B). We, however, also observed a smaller fraction of cells that showed osteopontin immunoreactivity while being immunonegative for Smi-32. Most of these cells were immunopositive for melanopsin (Figs. 3C, 3D), suggesting that these must be M1, M2, or M3 ipRGCs. While most of them had their soma in the ganglion cell layer, we found one cell with a rather weak osteopontin labeling residing in the inner nuclear layer. Of note, a small portion of osteopontin-positive cells was negative for both Smi32 and melanopsin,

Investigative Ophthalmology & Visual Science

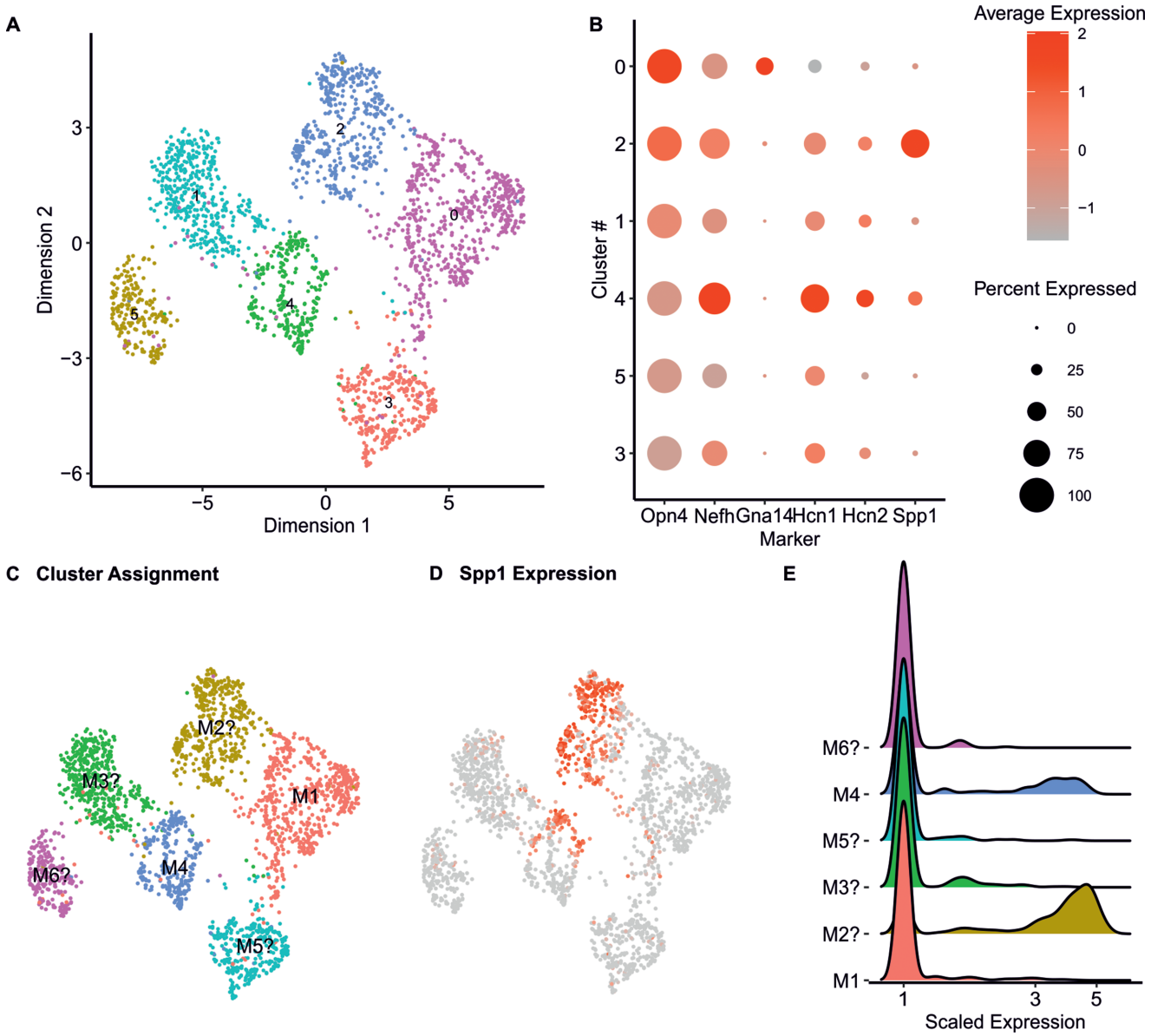

Figure 2. Transcriptomic expression patterns of Spp1 across ipRGC subtypes. Reanalysis of the Opn4-expressing cells from a publicly available sc RNA-seqdata set.[2] (**A**) Clustering and UMAP visualization after dimensionality reduction reveal six independent clusters of Opn4-expressing cells (#0–5). (**B**) Expression patterns of established markers were used to grossly annotate ipRGC subtypes.[3,16,27–29] (**C**, **D**) UMAP visualization as in (**A**) but with annotated clusters (**C**) and color-coded expression of Spp1 (**D**, *scale bar* as in **B**). (**E**) Ridgeline plot showing the distribution of Spp1 expression in the different clusters.

indicating the presence of other RGC types expressing also osteopontin.

To quantify the relative abundance of osteopontin-expressing M1 and M3 ipRGCs, we performed retinal flatmount staining, colabeling with melanopsin and osteopontin antibodies, and acquired confocal volume scans. On average, an area of 0.22 ± 0.04 mm^2 per retina (n = 5; 1.1 mm^2 in total) was analyzed. Through this double-labeling, we identified altogether 147 melanopsin-positive (M1–M3) ipRGCs and 143 osteopontin-positive cells. Seventy-eight cells colabeled for melanopsin and osteopontin, thus representing 53 % of all M1 to M3 ipRGCs. Performing confocal volume scans on these retinal flatmounts moreover allowed us to trace the dendritic arbor of individual cells, enabling us to determine dendritic stratification, which characteristically distinguishes between M1, M2, and M3 subtypes. Per flatmount stained, we traced the dendritic tree of one osteopontin$^+$/melanopsin$^+$ cell ("index") and one neighboring osteopontin$^-$/melanopsin$^+$ cell ("control"; n = 6 each). All index cells were monostratifying in the ON sublamina of the inner plexiform layer exclusively, suggesting they were M2 ipRGCs. By contrast, control cells were either monostratifying in the OFF layer or bistratifying in ON and OFF layers (Figs. 4, 5A), therefore most likely representing the ipRGC subtypes M1 (OFF) and M3 (ON–OFF). In agreement with these findings, we observed that the index cells had a large dendritic field diameter of 253.91 ± 20.3 µm and many (20 ± 3) dendritic branching points, while the control cells had a smaller dendritic field diameter of 243.47 ± 44.6 µm and fewer (12 ± 3) branching

Investigative Ophthalmology & Visual Science

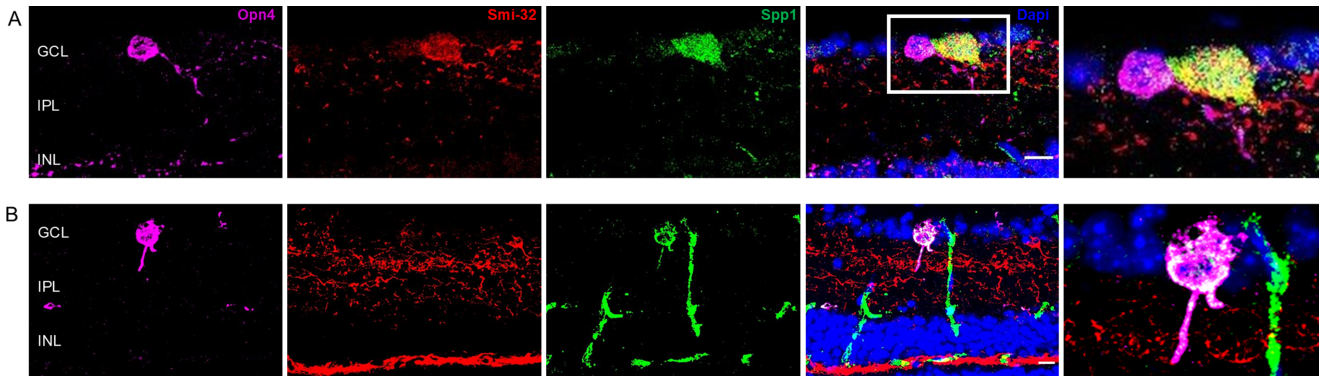

Figure 3. Osteopontin immunoreactivity in αRGCs and a subset of melanopsin-immunopositive ipRGCs. Confocal micrographs of retinal cryosections immunostained for melanopsin (=Opn4, *magenta*), neurofilament heavy chain protein (=Smi-32, *red*), and osteopontin (=Spp1, *green*). (**A**) Representative example of a cell where Spp1 immunoreactivity colocalizes with Smi-32 but not with Opn4. (**B**) Representative example of a cell where Spp1 immunoreactivity colocalizes with Opn4Smi-32 but not with Smi-32, most likely representing an M1, M2, or M3 ipRGC. Blood vessels showing up in the Spp1-channel (*green*) due to murine origin of the osteopontin antibody. INL, inner nuclear layer; IPL, inner plexiform layer. *Blue channel*: DAPI. *Scale bar*: 10 µm.

points (Figs. 5B, 5C). Also, in accordance with these findings, the mean intensity of the melanopsin immunofluorescence measured over the somata of index cells was significantly lower compared to that of control cells. As for the osteopontin intensity, there was moderately but significantly weaker signal in the osteopontin$^+$/melanopsin$^+$ cells compared to cells that only expressed osteopontin but no melanopsin (i.e., mostly αRGC; relative fluorescence intensity in osteopontin$^+$/melanopsin$^+$ was 73% [inter quartile range, 65%–79%] of that observed in osteopontin$^+$/melanopsin$^-$ cells; $P = 0.032$).

Discussion

In the present work, we provide an in-depth characterization of the expression pattern of osteopontin across ipRGC subtypes. Using transcriptomic and immunohistochemical techniques, we demonstrate that not only M4—as previously thought—but also M2 ipRGCs express osteopontin. In immunohistochemical experiments, double- labeling for osteopontin and melanopsin may therefore provide a method to identify and differentiate M2 ipRGCs (with clear melanopsin and high osteopontin immunoreactivity) from other subtypes. This will facilitate future studies aiming to dissect the functional roles of individual ipRGC subtypes.

To draw this conclusion, we commenced by analyzing the ipRGCs contained in a publicly available RNA-seq data set[2] and found osteopontin expression on two distinct clusters. Judged by the expression of αRGC marker Smi-32 and signal transduction genes differentially operative in M1 to M6 ipRGCs,[11,26,29] these clusters resembled M2 and M4 cells, respectively. Indeed, using immunohistochemical approaches, we were then able to confirm the existence of a Smi-32–negative (i.e., non-M4) population of cells that was mostly immunopositive for melanopsin. We could then show that this osteopontin$^+$/melanopsin$^+$ population exhibited structural features that are characteristic for the M2 subtype, most prominently, the ON lamina stratification of their dendritic tree.[9] Consistently, osteopontin$^+$/melanopsin$^+$ cells had a larger, more complex dendritic tree and expressed lower levels of melanopsin as compared to osteopontin-negative ipRGCs. Moreover, making up approximately 50% of all Opn4$^+$ cells, this proportion nicely matches that expected for M2—but was far too high for the alternative but rare M3 subtype.[30,31]

As mentioned above, osteopontin expression has been previously considered to be αRGC-exclusive, and studies have thus used osteopontin as a marker (or genetic selector) for this cell type.[15,17,32] The present study, as well as the results by Zhao et al.,[18] now show that this is indeed not fully precise. As a whole, αRGCs clearly outnumber M2-ipRGCs. However, if selecting αRGC by osteopontin expression, the systematic inclusion of M2 cells would induce an unwanted bias that could be more or less relevant depending on the specific experimental question.

In our immunohistochemical experiments, we also noticed a small portion of osteopontin-positive cells that expresses neither Smi-32 nor melanopsin. In theory, these cells could be a yet entirely different type of RGC or any of the two other ipRGC subtypes (besides M4) with melanopsin expression levels too low for immunohistochemical detection (i.e., either M5 or M6). From our transcriptomic analyses, it appears likely that these cells were rather not M5 or M6, as the clusters representing these subtypes yielded expression level of *Spp1* that were virtually zero.

One additional observation we made is that on transcriptomic-level *Spp1*, expression was even higher in the M2 cluster than in the M4 cluster. We were not able to test if that observation was preserved to protein level, as we did not distinguish between M4 and the other Smi-32–positive αRGCs in IHC. Yet, based on the transcriptomic results alone, it would seem that in fact, M2 cells might be those with the strongest osteopontin expression among the ipRGCs. Notably, this does not mean that M2 osteopontin levels would exceed those of all other RGC types in general; rather, our immunostaining experiments indicate that osteopontin levels are lower in M2 cells than in the overall αRGC population (i.e., osteopontin expression M4 < M2 < non-M4-αRGC).

In this study, we aimed to characterize the expression patterns of osteopontin across ipRGCs, considering osteopontin as a cellular marker, while its functional role in these cells has not been our focus. Interestingly, osteopontin had

Investigative Ophthalmology & Visual Science

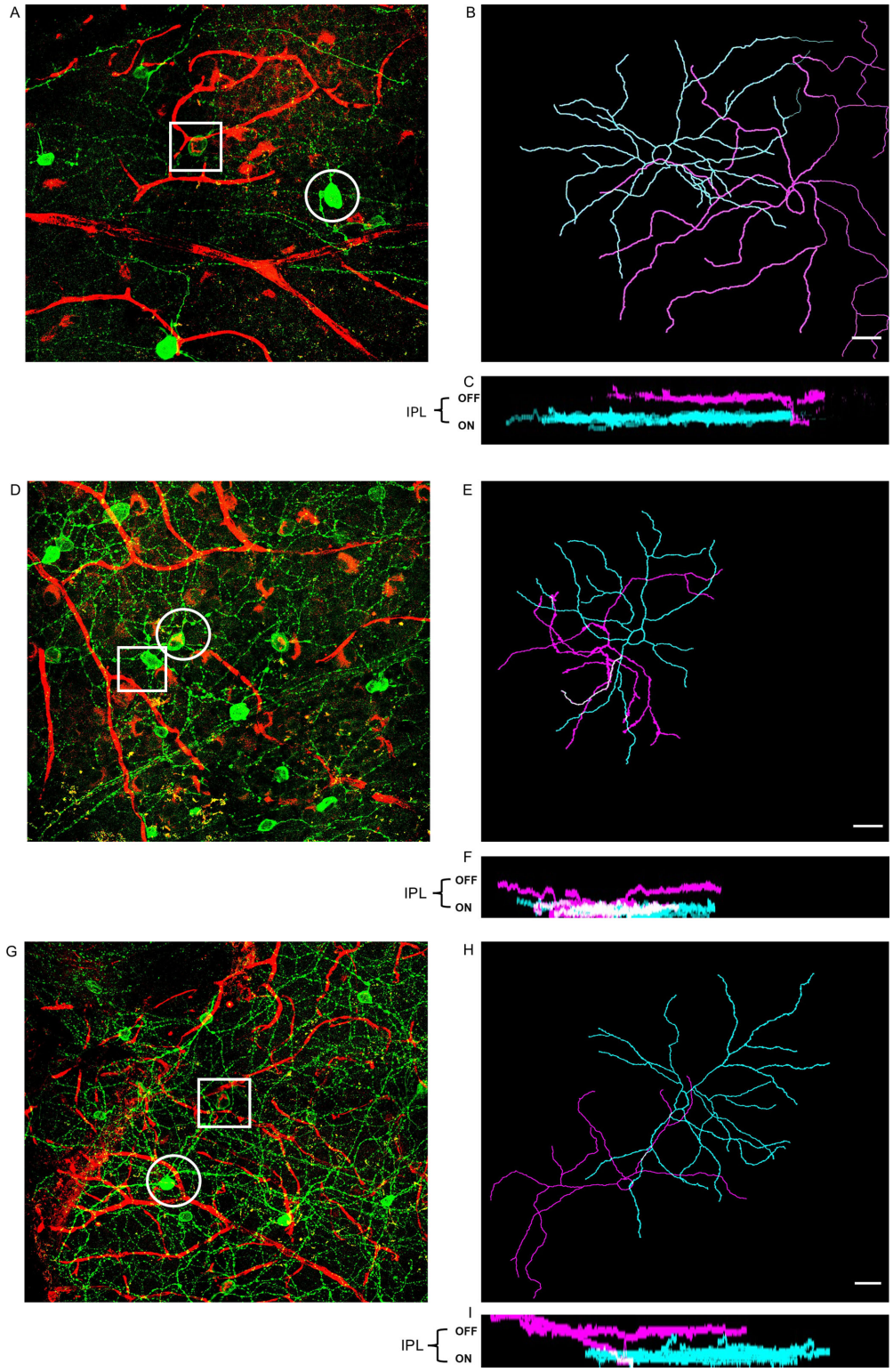

Figure 4. Osteopontin immunoreactive ipRGCs structurally resemble M2 cells. (**A**, **D**, **G**) Exemplary Z-projections of confocal volume scans from murine retinal flatmounts immunolabeled for osteopontin (*red*) and melanopsin (*green*). Osteopontin^{+}/melanopsin^{+} ipRGC ("index-cell," *square*) next to osteopontin^{-}/melanopsin^{+} ipRGCs ("control-cell," *circle*). (**B**, **E**, **H**) Outlines of neurite-traced neurons: osteopontin^{+}/melanopsin^{+} index cell (*cyan*) next to osteopontin^{-}/melanopsin^{+} control cell (*magenta*). (**C**, **F**, **I**) Orthogonal representation of the traced cells showing the index cells monostratifying in the ON sublayer of the IPL and control cells either monostratifiying in the OFF layer (**C**, **I**) or bistratifying in ON and OFF sublayers of IPL (**F**). Blood vessels showing up in the osteopontin channel (*green*) due to murine origin of the osteopontin antibody. *Scale bar*: 30 µm.

Investigative Ophthalmology & Visual Science

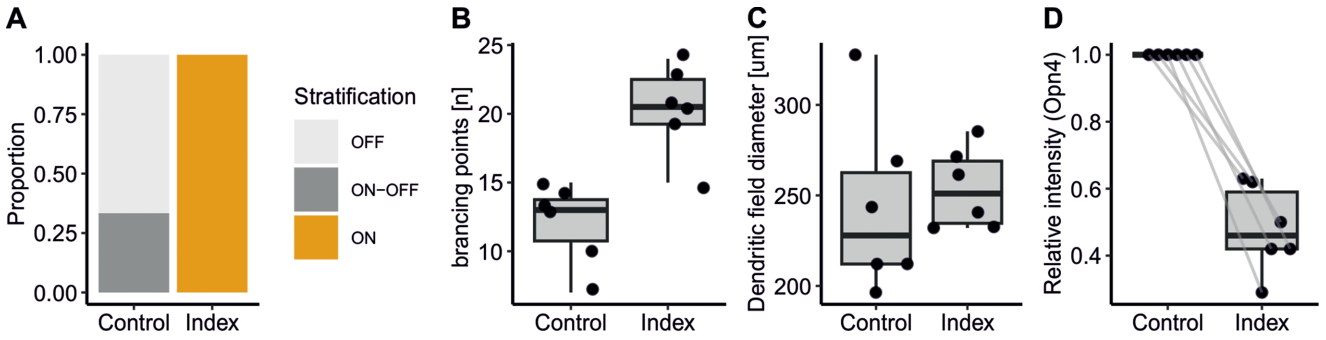

Figure 5. Statistical analysis of morphologic characteristics found in traced index and control cells. (**A**) Stratification patterns of osteopontin$^+$/melanopsin$^+$ ("index") and osteopontin$^-$/melanopsin$^+$ ("control") cells, showing index cells stratifying exclusively in the ON sublamina of the IPL, while traced control cells were monostratifying in the OFF sublayer (66,66%) and bistratifying in ON and OFF layers (33.33%). (**B**) Average number of branching points of index and control cells showing a more complex dendritic arborization of our index cells along with a larger dendritic field diameter as shown in (**C**). (**D**) Relative pixel intensity in the melanopsin (Opn4) channel from the index cell in relation to the respective control cells. Index cells show a significantly lower melanopsin signal intensity.

been suggested to render RGCs resilient to (axonal) injury or other damage. Possibly this concept might have been led by the strong overlap between the cells belonging to the group of αRGCs and those expressing osteopontin. Indeed, it has been shown that osteopontin supports RGC survival, possibly in an interplay with insulin-like growth factor receptor 1. Yet, while supportive, it is clearly not essential for it.[15] On the other end, more recent results based on data-driven techniques demonstrate that resilience is predominantly a feature of ipRGCs rather than αRGCs, and while transcriptomic determinants for RGC resilience can be identified, *Spp1* is not one of those genes with the strongest effect.[2] Still, the refined characterization of osteopontin expression across ipRGC subtypes provided herein will support attempts to identify therapeutically usable factors supporting RGC survival and resilience, such as promoted by the RReSTORe consortium.[33]

The approach chosen in this study, starting from subsetting ipRGCs by *Opn4* expression from a large transcriptomic data set,[2] has enabled us to robustly cluster this relatively rare set or retinal neurons. While we have used this approach to assess the expression patterns of *Spp1*/osteopontin herein, it can also serve as a more general approach for identifying ipRCG subtype markers in future studies. For such purposes, other large single-cell data sets, like that published by Rheaume et al.,[34] may serve as a reference to narrow down the list of candidate markers. For characterizing the expression pattern of one particular marker, in this study, we performed in-depth structural characterization of osteopontin$^+$/melanopsin$^+$ (and osteopontin$^-$/melanopsin$^+$ control cells) for a relatively small number of samples using manual neurite tracing. While the relatively small sample size might be somewhat of a limitation to this study, observing the characteristic M2 ON-sublamina stratification in 100% of the index and 0% of the control cells, together with the observation that all other morphometric measures fitted well into this hypothesis, does provide a high degree of confidence that our findings were indeed robust.

In conclusion, in the present study, we can demonstrate that osteopontin is expressed in two distinct subtypes of ipRGCs, namely, M2 and M4 cells. The combination of high osteopontin and clear melanopsin immunoreactivity may thereby facilitate the identification of M2 ipRGCs.

Acknowledgments

The authors thank Burkhard Schütz and the Department of Anatomy for providing access to their cryotome.

Supported by the German Research Foundation (LI 2846/5-1 and LI 2846/6-1 to ML).

Author Contributions: Participated in researchdesign: LK, ML; Conducted experiments: LK; Performed data analysis: LK, ML; Wrote or contributed to the writing of the manuscript: LK, ML.

Ethics Approval: This study did not involve human participants. Animal work was performed with approval of the relevant authorities and in accordance with the institutional Ethics Guidelines of Animal Care. Further details are provided in the Methods section.

Data Availability: The data sets generated and/or analyzed during the current study are available from the corresponding author on reasonable request.

Disclosure: **L. Kinder**, None; **M. Lindner**, Bayer Healthcare (F)

References

1. Baden T, Berens P, Franke K, Roman Roson M, Bethge M, Euler T. The functional diversity of retinal ganglion cells in the mouse. *Nature*. 2016;529:345–350.
2. Tran NM, Shekhar K, Whitney IE, et al. Single-cell profiles of retinal ganglion cells differing in resilience to injury reveal neuroprotective genes. *Neuron*. 2019;104:1039–1055.e1012.
3. Schmidt TM, Alam NM, Chen S, et al. A role for melanopsin in alpha retinal ganglion cells and contrast detection. *Neuron*. 2014;82:781–788.
4. Berson DM, Dunn FA, Takao M. Phototransduction by retinal ganglion cells that set the circadian clock. *Science*. 2002;295:1070–1073.
5. Hattar S, Liao HW, Takao M, Berson DM, Yau KW. Melanopsin-containing retinal ganglion cells: architecture, projections, and intrinsic photosensitivity. *Science*. 2002;295:1065–1070.
6. Hattar S, Lucas RJ, Mrosovsky N, et al. Melanopsin and rod-cone photoreceptive systems account for all major accessory visual functions in mice. *Nature*. 2003;424:76–81.

7. Aranda ML, Schmidt TM. Diversity of intrinsically photosensitive retinal ganglion cells: circuits and functions. *Cell Mol Life Sci*. 2021;78:889–907.
8. Kinder L, Palumaa T, Lindner M. Intrinsically photosensitive retinal ganglion cells. *Ophthalmologe*. 2022;119:358–366.
9. Sondereker KB, Stabio ME, Renna JM. Crosstalk: the diversity of melanopsin ganglion cell types has begun to challenge the canonical divide between image-forming and non-image-forming vision. *J Comp Neurol*. 2020;528:2044–2067.
10. Chen SK, Badea TC, Hattar S. Photoentrainment and pupillary light reflex are mediated by distinct populations of ipRGCs. *Nature*. 2011;476:92–95.
11. Sonoda T, Lee SK, Birnbaumer L, Schmidt TM. Melanopsin phototransduction is repurposed by ipRGC subtypes to shape the function of distinct visual circuits. *Neuron*. 2018;99:754–767.e754.
12. Quattrochi LE, Stabio ME, Kim I, et al. The M6 cell: a small-field bistratified photosensitive retinal ganglion cell. *J Comp Neurol*. 2019;527:297–311.
13. Stabio ME, Sabbah S, Quattrochi LE, et al. The M5 cell: a color-opponent intrinsically photosensitive retinal ganglion cell. *Neuron*. 2018;97:150–163.e154.
14. Yim A, Smith C, Brown AM. Osteopontin/secreted phosphoprotein-1 harnesses glial-, immune-, and neuronal cell ligand-receptor interactions to sense and regulate acute and chronic neuroinflammation. *Immunol Rev*. 2022;311:224–233.
15. Duan X, Qiao M, Bei F, Kim IJ, He Z, Sanes JR. Subtype-specific regeneration of retinal ganglion cells following axotomy: effects of osteopontin and mTOR signaling. *Neuron*. 2015;85:1244–1256.
16. Krieger B, Qiao M, Rousso DL, Sanes JR, Meister M. Four alpha ganglion cell types in mouse retina: function, structure, and molecular signatures. *PLoS One*. 2017;12:e0180091.
17. Gallego-Ortega A, Norte-Munoz M, Di Pierdomenico J, et al. Alpha retinal ganglion cells in pigmented mice retina: number and distribution. *Front Neuroanat*. 2022;16:1054849.
18. Zhao M, Toma K, Kinde B, et al. Osteopontin drives retinal ganglion cell resiliency in glaucomatous optic neuropathy. *Cell Rep*. 2023;42:113038.
19. Li S, Jakobs TC. Vitamin C protects retinal ganglion cells via SPP1 in glaucoma and after optic nerve damage. *Life Sci Alliance*. 2023;6(8):e202301976.
20. Lindner M, Gilhooley MJ, Palumaa T, Morton AJ, Hughes S, Hankins MW. Expression and localization of Kcne2 in the vertebrate retina. *Invest Ophthalmol Vis Sci*. 2020;61:33.
21. Schindelin J, Arganda-Carreras I, Frise E, et al. Fiji: an open-source platform for biological-image analysis. *Nat Methods*. 2012;9:676–682.
22. Preibisch S, Saalfeld S, Tomancak P. Globally optimal stitching of tiled 3D microscopic image acquisitions. *Bioinformatics*. 2009;25:1463–1465.
23. Arshadi C, Gunther U, Eddison M, Harrington KIS, Ferreira TA. SNT: a unifying toolbox for quantification of neuronal anatomy. *Nat Methods*. 2021;18:374–377.
24. Butler A, Hoffman P, Smibert P, Papalexi E, Satija R. Integrating single-cell transcriptomic data across different conditions, technologies, and species. *Nat Biotechnol*. 2018;36:411–420.
25. R Core Team. *R: A Language and Environment for Statistical Computing*. Vienna, Austria: R Project for Statistical Computing; 2018.
26. Jiang Z, Yue WWS, Chen L, Sheng Y, Yau KW. Cyclic-nucleotide- and HCN-channel-mediated phototransduction in intrinsically photosensitive retinal ganglion cells. *Cell*. 2018;175:652–664.e612.
27. Lin B, Wang SW, Masland RH. Retinal ganglion cell type, size, and spacing can be specified independent of homotypic dendritic contacts. *Neuron*. 2004;43:475–485.
28. Coombs J, van der List D, Wang GY, Chalupa LM. Morphological properties of mouse retinal ganglion cells. *Neuroscience*. 2006;140:123–136.
29. Chen L, Li G, Jiang Z, Yau KW. Unusual phototransduction via cross-motif signaling from G(q) to adenylyl cyclase in intrinsically photosensitive retinalganglion cells. *Proc Natl Acad Sci USA*. 2023;120:e2216599120.
30. Berson DM, Castrucci AM, Provencio I. Morphology and mosaics of melanopsin-expressing retinal ganglion cell types in mice. *J Comp Neurol*. 2010;518:2405–2422.
31. Hughes S, Watson TS, Foster RG, Peirson SN, Hankins MW. Nonuniform distribution and spectral tuning of photosensitive retinal ganglion cells of the mouse retina. *Curr Biol*. 2013;23:1696–1701.
32. Gallego-Ortega A, Vidal-Villegas B, Norte-Munoz M, et al. 7,8-Dihydroxiflavone maintains retinal functionality and protects various types of RGCs in adult rats with optic nerve transection. *Int J Mol Sci*. 2021;22(21):11815.
33. Soucy JR, Aguzzi EA, Cho J, et al. Retinal ganglion cell repopulation for vision restoration in optic neuropathy: a roadmap from the RReSTORe Consortium. *Mol Neurodegeneration*. 2023;18:64.
34. Rheaume BA, Jereen A, Bolisetty M, et al. Single cell transcriptome profiling of retinal ganglion cells identifies cellular subtypes. *Nat Commun*. 2018;9:2759.

Investigative Ophthalmology & Visual Science